Mn^{2+}-induced substitutional structural changes in ZnS nanoparticles as observed from positron annihilation studies

2008 J. Phys.: Condens. Matter 20 235226

(http://iopscience.iop.org/0953-8984/20/23/235226)

J. Phys.: Condens. Matter **20** (2008) 235226 (10pp) doi:10.1088/0953-8984/20/23/235226

Mn^{2+}-induced substitutional structural changes in ZnS nanoparticles as observed from positron annihilation studies

Subhajit Biswas[1,3], Soumitra Kar[1,3], Subhadra Chaudhuri[1,4] and P M G Nambissan[2]

[1] Department of Materials Science, Indian Association for the Cultivation of Science, Kolkata 700032, India
[2] Nuclear and Atomic Physics Division, Saha Institute of Nuclear Physics, 1/AF Bidhannagar, Kolkata 700064, India

E-mail: pmg.nambissan@saha.ac.in

Received 13 November 2007, in final form 13 April 2008
Published 9 May 2008
Online at stacks.iop.org/JPhysCM/20/235226

Abstract

Zinc sulfide nanoparticles doped with different concentrations of manganese ions (Mn^{2+}) were synthesized at various temperatures to investigate the effects of substitution and the associated defect evolution. Positron lifetime and Doppler broadening measurements were used as probes. The initial stage of defect recovery was dominated by the occupation of Zn^{2+} vacancies by Mn^{2+} ions, bringing in characteristic changes in the positron lifetimes, intensities and Doppler broadened lineshape parameters. Detailed analyses considering the presence of one and two types of defects were carried out to identify the type of defects which trap positrons at the different dopant concentrations. Electron paramagnetic resonance studies indicated increased Mn–Mn interaction and the formation of Mn clusters with further doping. The results are in striking contrast to those for nanorods, where vacancy recombination transformed their interior into regions free of defects.

1. Introduction

Studies of nanocrystalline systems of semiconductor materials are of interest for a wide range of applications, both physical and technological, due to the remarkable improvement in their properties as well as the interesting processes related to their synthesis and characterization. Quantum confinement effects and different structural transitions have been reported in the case of several such nanomaterials and deeper insights into these aspects have been called for [1–3]. In our recent works [3–5] we have focused on the structural defects associated with grains and rods of semiconductor nanomaterials and some useful information about their structure and properties has been highlighted. The technological importance of ZnS is widely known. It is a very popular material for applications in optoelectronic devices and sensors, apart from its other uses in photoconductors, phosphors and electroluminescent materials. Because of its wide band gap (3.75 eV), it is also put to use for gathering information on the changes in properties due to doping by different elements. Manganese normally occupies the substitutional sites in the Zn lattice as divalent ions and the excitation and decay of this ion have been seen to produce luminescence features at characteristic wavelengths [1, 2, 4]. The incorporation of Mn^{2+} ions has been shown to effect a structural transition to the cubic phase in the case of ZnS nanorods synthesized with an initial hexagonal structure [4, 6]. In a recent positron annihilation study of Mn-doped ZnS nanorods [6] we argued that the interior of the nanorods became free of vacancy-like defects due to the doping and the positrons either annihilate in the bulk or at the surfaces of the nanorods. In this work we report the results of studies on zinc sulfide nanoparticles with a cubic zincblende structure and doped with different concentrations of manganese ions at different temperatures, and examine the positron annihilation characteristics pertaining to the processes of defect evolution.

[3] Present address: NanoScience Technology Center, University of Central Florida, Orlando, FL-32826, USA.
[4] Deceased.

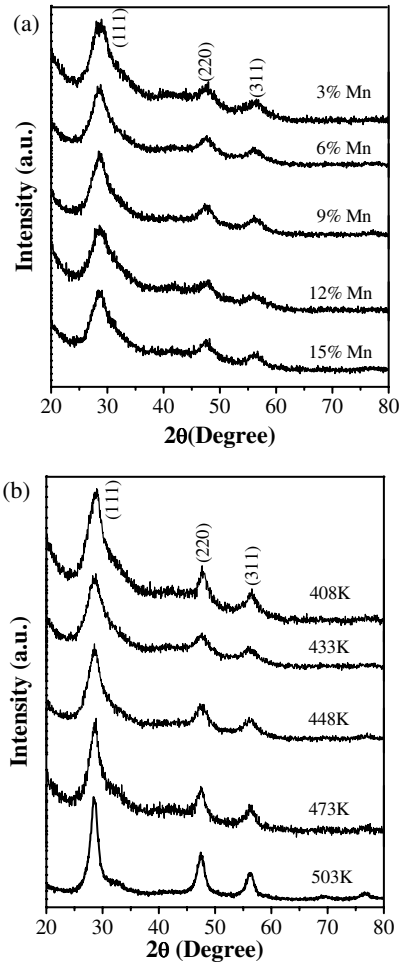

Figure 1. X-ray diffraction patterns of the Mn-doped ZnS nanoparticles (a) at different dopant concentrations and (b) synthesized at different temperatures.

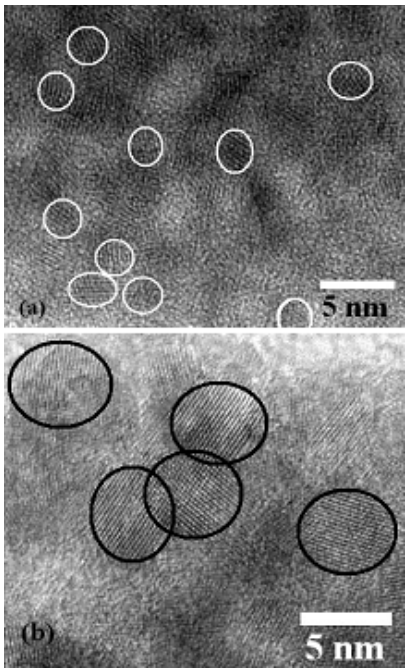

Figure 2. High-resolution transmission electron micrograph of ZnS nanoparticles synthesized at two different temperatures: (a) 433 K and (b) 473 K.

2. Experimental section

$Mn_xZn_{1-x}S$ nanoparticles were synthesized using a normal solvothermal process. Appropriate amounts of zinc acetate ($(CH_3COO)_2Zn{\cdot}4H_2O$), manganese acetate ($(CH_3COO)_2Mn{\cdot}4H_2O$) and thiourea ($NH_2CSNH_2$) were taken in a Teflon-lined cylindrical stainless steel chamber. The chamber was filled with ethanol up to 80% of its volume. Thiourea was used at three times the stoichiometric ratio. After stirring for 30 min, the closed chamber was placed inside a box furnace at the desired temperature for 12 h and then slowly cooled down to room temperature. The white precipitate was filtered off and washed several times in water and ethanol. The final product was dried in a vacuum at 353 K for 6 h to get a white powder.

Two sets of samples were prepared. In the first set, there were eight samples synthesized at the same temperature (433 K) but each with a different input Mn^{2+} concentration varying from 0.05 to 30 at.%. In the second set, the input Mn^{2+} concentration is fixed at 6 at.% but the five samples were synthesized at five different temperatures, i.e. 408, 433, 448, 473 and 503 K. The purpose was to examine the consequent effects of incorporation of Mn^{2+} ions in the ZnS lattice and possible variations due to change of temperature (i.e. with the change of particle size).

The products were analyzed using an x-ray diffractometer (XRD; Seifert 3000P) with Cu Kα radiation and the compositional verification was done by energy dispersive x-ray analysis (EDAX; Kevex, Delta class I). A few representative x-ray diffraction patterns are shown in figures 1(a) and (b). The manifestation of the diffraction peaks with distinguishable sharpness ensures that a certain crystalline order still prevails within the grains despite the very small sizes. From the size of the particles estimated from x-ray diffraction patterns of samples synthesized at the same temperature, we have seen that the grain sizes did not vary considerably due to Mn^{2+} doping and all the grains had a size of about 2.5 nm. The microstructures and crystallinity of the samples were further confirmed using transmission electron microscopy (TEM) and high-resolution TEM (HRTEM; JEOL 2010) studies (figures 2(a) and (b)). Electron paramagnetic resonance (EPR) studies of the powder samples were done with a Varian E-109C X-band spectrometer.

Positron lifetime measurements were carried out with a ^{22}Na source (400 kBq) in thin nickel foil immersed in the powdered samples and the spectra were recorded using a slow–fast gamma–gamma coincidence set-up with prompt time resolution (full width at half maximum) 200 ps under experimental settings. The sample and source were kept in dry vacuum conditions in order to ensure the removal of any traces of air trapped within the powder and otherwise adsorbed gases (see discussion later). About (1.5–2.0) $\times$ 10^6 counts were collected under each spectrum with a peak to background ratio better than 10 000:1, and the data were analyzed using the programs RESOLUTION and POSITRONFIT [7]. For

Doppler broadening measurements, a HPGe detector with resolution 1.14 keV at 511 keV was used. For coincidence Doppler broadening (CDBS) measurements, one more similar detector with identical resolution was used in the anticollinear direction and the two parameter spectra, each comprising about 7×10^6 counts, were recorded and analyzed using the standard procedure [8].

3. Results and discussions

The actual values of positron lifetimes in pure undoped ZnS nanocrystalline samples vary with the average particle or grain size. In an earlier work [5] we obtained $\tau_1 = 147$ ps and $\tau_2 = 380$ ps with respective relative intensities $I_1 = 43.6\%$ and $I_2 = 44.0\%$ for a sample of grain size close to the present size (∼2 nm). (All the values shown against $x = 0.01$ at.% in the figures shown hereafter represent the undoped sample.) The presence of yet another and still longer lifetime $\tau_3 = 2.10$ ns of intensity $I_3 = 12.4\%$ was attributed to the formation of orthopositronium atoms, the temporary bound state of positrons with electrons before eventual annihilation, in free volume cavities (or defects) [9]. The two shorter lifetimes τ_1 and τ_2 indicate that positrons are also trapped in defects other than these regions. A small contribution to the measured values of τ_1 in all the samples also comes from parapositronium atoms with an intrinsic lifetime 125 ps and intensity one-third of I_3, but the qualitative variation of τ_1 either with the Mn^{2+} ion concentration or temperature of synthesis of the samples was found to be unaffected and hence is not explicitly shown or stated hereafter.

ZnS is known to contain large number of Zn^{2+} vacancies and, owing to their negative charge, positrons should experience additional attraction (with respect to neutral vacancies) towards them. The value of $\tau_2 = 380$ ps is higher than the positron lifetime of 233 ps in Zn^{2+} monovacancies (V_{Zn}) of bulk coarse-grained ZnS, as reported by Plazaola *et al* [10] and Brunner *et al* [11], although Adams *et al* [12] had mentioned a relatively high value of 290 ps. The higher value of τ_2 in the present work is consistent with the fact that the samples are composed of nanoparticles and a significant fraction of the positrons annihilate in the vacancy-type defects on the grain surfaces. This argument is based on the fact that the grain size of 2.5 nm of the samples used here is significantly less than the typical thermal diffusion lengths of positrons (50–100 nm [13]) and hence the thermalized positrons can diffuse out to the surface of grains prior to annihilation. Another reason for the larger values of the obtained positron lifetimes is that the grain size of 2.5 nm is smaller than the excitonic Bohr diameter of ZnS (∼5 nm [14]). This means that quantum confinement effects have already set in and given rise to the average one electron energy level split and an effective increase in the band gap in the atoms of these grains. The positron lifetimes in such cases, for example the one reported by us on CdS, have been shown to increase due to the reduced annihilation probabilities [3].

Compositional analysis of the $Mn_xZn_{1-x}S$ nanostructures was initially carried out by EDAX analysis. The results for the sample with a Mn^{2+} concentration of 6 at.% are shown in figure 3. In pure ZnS, elemental Zn and S were found in near-stoichiometric ratio. The EDAX spectra of one representative Mn doped ZnS sample is shown in the inset of figure 3. In the Mn-doped ZnS samples, the amount of Mn^{2+} detected by the EDAX analysis was less than that actually added during the synthesis. However, the actual intake of Mn^{2+} increases with increasing synthesis temperature, as shown in the figure. Since EDAX is not suitable for detecting very low concentration of dopants, it is very difficult to estimate the actual Mn^{2+} percentage for the samples synthesized with a very low concentration of input manganese (0.05–1 at.%), although the presence of Mn^{2+} ions within the ZnS host lattice of these samples was confirmed by EPR studies, as discussed later. Therefore, we subsequently still use the input Mn^{2+} concentration as the experimental variant for qualitative interpretation of the results. With the inclusion of Mn^{2+} ions in the lattice, the shorter lifetime τ_1 decreases while τ_2 increases from 380 to 395 ps (figure 4). The intensity I_2 surprisingly reduces drastically, indicating significant annulment of a certain species of defects present in the samples. An increasing τ_2 with a rapidly diminishing I_2 could be possible when a fraction of vacancy-type defects, especially of relatively smaller sizes, are compensated by the input Mn^{2+} ions. The τ_2 then resulting from the remaining defects and overwhelmingly from the grain surfaces would be averaged to a higher value, as shown in figure 4. The values of τ_2 at further increasing concentrations of Mn^{2+} did not exhibit any systematic variation and were scattered (within error bars) around a mean value of 395 ps. In the final analysis, the results of which are reported here, therefore, τ_2 was fixed at 395 ps (figure 4). As mentioned earlier, the main contribution to τ_2 in the Mn-doped samples is the annihilation of positrons at the grain surfaces, and it can be influenced only by the volume or size of the defects present there. The fractional excess free volume of a defect at the grain surface, in turn, depends only on the size of the grains and hence that essentially remains the

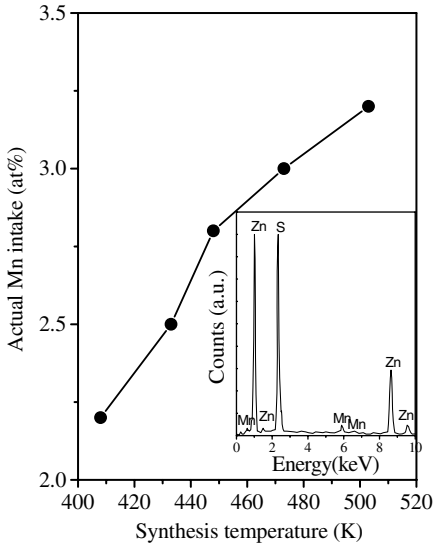

Figure 3. The actual concentration of Mn^{2+} ions being substituted inside the 6 at.% Mn-doped sample synthesized at different temperatures, as obtained from the EDAX analysis. The EDAX spectrum of one of the samples is shown in the inset.

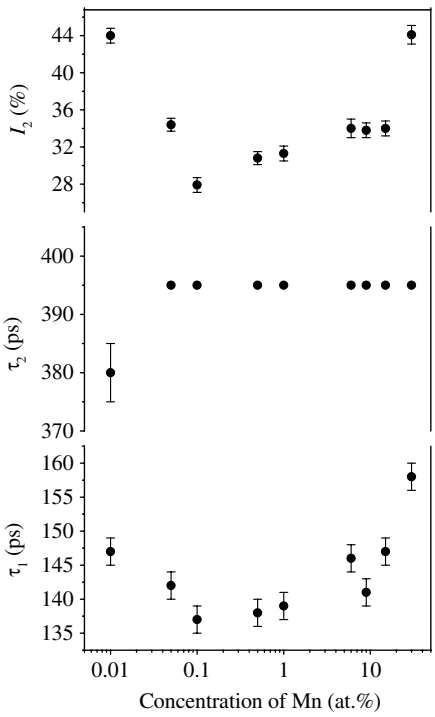

Figure 4. The variation of the positron lifetimes τ_1 and τ_2 and the intensity I_2 with Mn^{2+} concentration in the ZnS nanoparticles. The data points corresponding to the undoped (x coordinate = 0) sample are shown against 0.01 at.%.

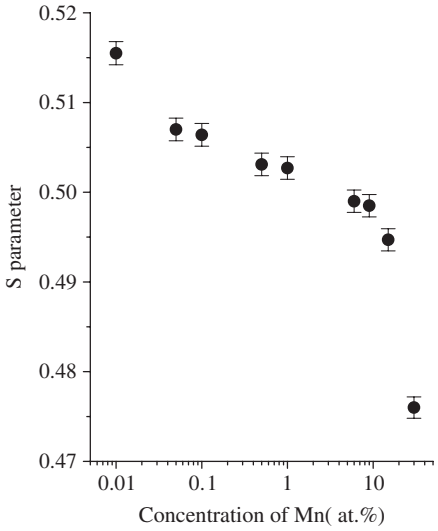

Figure 5. The S parameter versus the Mn^{2+} concentration of the ZnS nanoparticles. The data points corresponding to the undoped (x coordinate = 0) sample are shown against 0.01 at.%.

same if the grain size does not change [15]. As already stated, the latter aspect has been verified in this case through x-ray diffraction and TEM studies and the grain sizes of samples with different Mn^{2+} concentrations were all around 2.5 nm. No changes in the case of τ_2 are therefore expected.

Simultaneous measurements of the Doppler broadening of the positron annihilation gamma ray spectrum offer another complementary support for the interpretations presented above. The changes are monitored in terms of the lineshape parameter denoted by S, which is defined as the ratio of counts falling under an energy window of ± 0.8 keV around the peak (511 keV) to the total counts under the whole spectrum, after subtraction of the nuclear gamma ray background. The S parameter, when shown as varying with the inclusion of Mn^{2+} in at.% (figure 5) also reveals a distinct defect recovery stage with the inclusion of Mn^{2+} ions. The initial decrease of S supports the dominant process of recombination of the vacancy-type defects with the doped Mn^{2+} ions, although a major influence on the behavior of S can come from the percentage of positronium atoms formed, as discussed later. The recombination process continues until the dopant concentration reaches 1 at.% and is indicated by rather smooth changes in the annihilation parameters up to this concentration.

For ZnS with an acceptor-type defect like V_{Zn}, the arrival of a Mn^{2+} ion would immediately help to compensate the missing holes. Since pure ZnS normally turns out to be sulfur deficient, the formation of antisite defects (S_{Zn}) can be ruled out. Also since the sulfur vacancies are positively charged, they cannot trap positrons. The results of CDBS experiments illustrated in figures 6(a), (b) and (c) support this argument. In order to generate the ratio curves, the area-normalized counts of the corresponding spectra were divided by those of the spectrum of a pure annealed aluminum sample [8]. The peak of the curve representing the undoped ZnS coincides with that of elemental sulfur, suggesting that positrons are essentially annihilating from the vacancies of zinc. With the inclusion of Mn^{2+} ions, there are characteristic changes and these are discussed later.

The positron lifetime (τ_f) measured in the bulk coarse-grained ZnS is 215 ps, which is close to the values widely reported in the literature for cubic ZnS (~217–227 ps) [10–12]. The nanocrystalline samples are expected to contain defects, both inside the grain and on the outside surfaces. As in the case of nanorods [6], the number of different types of defects present in the nanoparticle samples under investigation can be assessed by using the trapping model equations [16, 17] and cross-checking the estimated positron lifetime τ_1 with its experimentally measured value. The trapping model assumes a delocalized state of positrons diffusing in the bulk region of the crystal besides the trapped states. In nanocrystalline grains of sizes much smaller than the thermal diffusion lengths of positrons, the 'bulk' state is attributed to those positrons, which do not eventually reach the surface but continue diffusion within the grains until annihilation takes place. The simplest case of the trapping model assumes just one type of defect [16], say if we assume that the interiors of the nanocrystalline grains are free of crystal vacancies and only the grain surfaces trap positrons. This, however, did not yield agreement between the calculated and experimentally measured values of τ_1. Hence the values were also calculated using the three-state trapping model [17], in which the longer lifetime τ_2 is considered as correctly resolved and the possibility of positron trapping in other types of defects is explored by comparing the experimental lifetime τ_1 with that obtained from

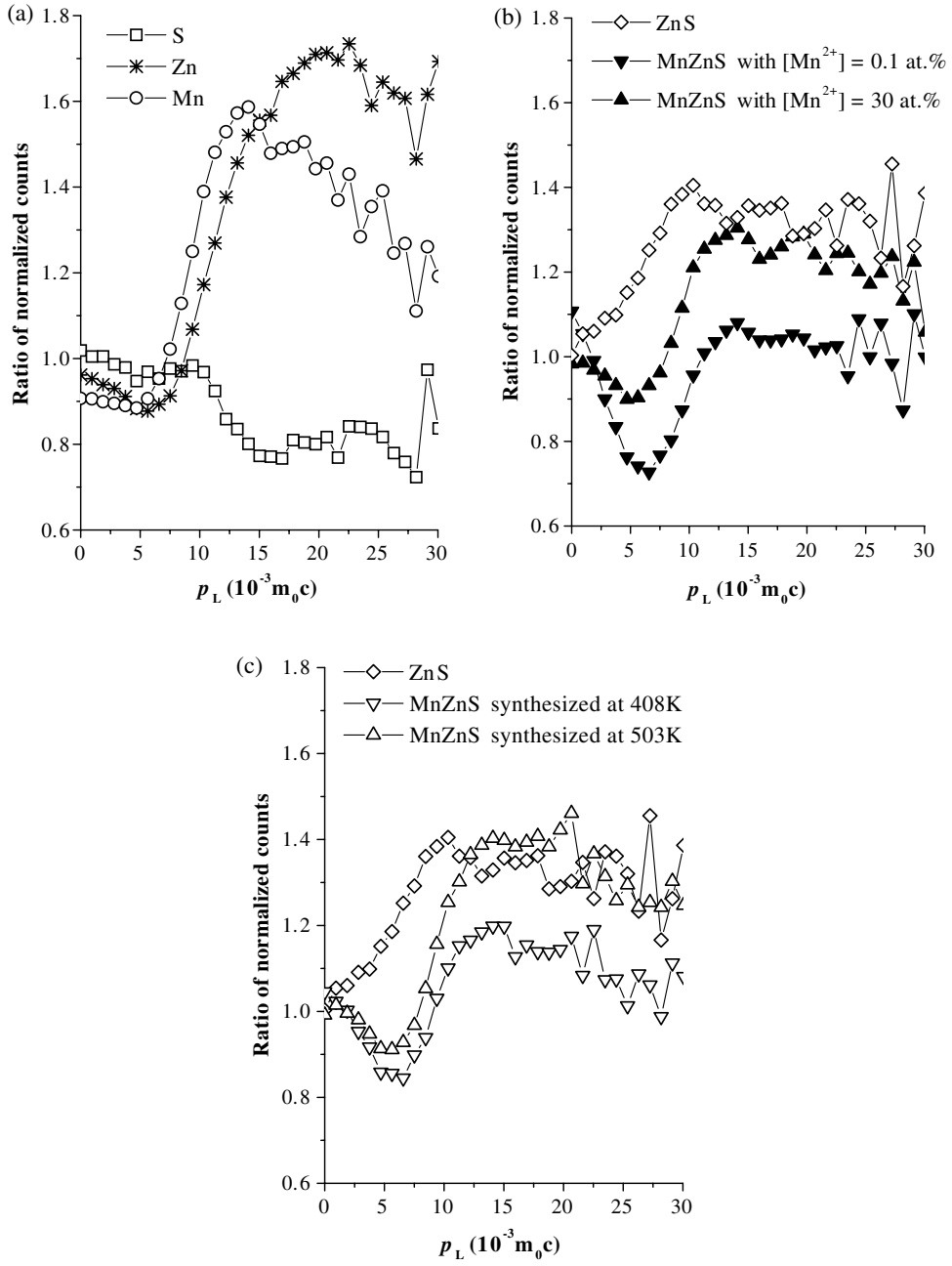

Figure 6. The quotient spectra obtained by dividing the coincidence Doppler broadened spectra of some of the samples—(a) of elements S, Zn and Mn, (b) ZnS and Mn-doped ZnS with different Mn^{2+} ion concentrations and (c) ZnS and Mn-doped ZnS of different temperatures of synthesis—by the spectra of a pure Al sample.

the equation [17]

$$\tau_1^{\text{cal}} = \frac{1 + \frac{\kappa_1}{\lambda_1}\left(1 + \frac{\kappa_2}{\lambda_f - \lambda_2 + \kappa_1}\right)}{\lambda_f + \kappa_1 + \kappa_2}. \quad (1)$$

In this equation, the annihilation rates λ_f and λ_1 are just the reciprocals of the respective lifetimes τ_f and τ_1 and κ_1 and κ_2 (described afterward) are the rates of trapping of positrons into the two types of defects under consideration. In all these calculations, both in the two-state and three-state trapping models, the weighted average of τ_2 and the positronium lifetime τ_3 are used in place of τ_2 in the appropriate equations [16, 17]. This is justified since positronium is formed by a fraction of the positrons which are trapped in the defects on the grain surfaces. (Although positronium formation is not generally reported for metallic or semiconductor systems of the macroscopic grain size owing to the high electron densities involved, there is a distinct possibility for the same in the case of nanomaterial systems as the grain surfaces and interfaces are sites of very low electron density and which can probably act as favorable sites for a fraction of the positrons to form positronium.) The agreement between the calculated and measured values of τ_1 was found satisfactory only in the two extreme cases, i.e. the undoped sample and the sample

Table 1. The experimentally measured and calculated values of τ_1 in samples with different input concentration of Mn^{2+} ions. τ_1^{cal-3a} refers to the values obtained from the three-state trapping model (equation (1)) and τ_1^{cal-3b} to those from the three-state trapping model (equation (2)). The typical error is ±2 ps.

Conc. of Mn^{2+} (%)	τ_1^{exper} (ps)	τ_1^{cal-3a} (ps)	τ_1^{cal-3b} (ps)
0	147	147	96
0.05	142	163	129
0.1	137	181	144
0.5	138	172	133
1	139	176	147
6	146	167	139
9	141	168	138
15	147	169	146
30	158	157	141

with a Mn^{2+} concentration of 30 at.%. The results thus indicated that these samples basically contained two kinds of positron trapping sites. Besides the diffused vacancies on the nanocrystalline grain surfaces, the undoped ZnS nanoparticles contained crystal vacancies, the majority of which get occupied by the Mn^{2+} ions on doping. The shorter lifetime τ_1 also decreases at this stage. τ_1 is a result of trapping of positrons from the delocalized Bloch state into the defects and is always admixed with the lifetime of the positrons annihilating in the defect-free region. Consistent with equation (1), its values should be always less than τ_f, as shown in table 1. It may be argued that, owing to the nanometer size of the grains and the thermal diffusion of the positrons, nearly all the positrons should reach the surfaces of the grains before annihilation. Such a situation would have given a saturation lifetime of 230 ps or more for all the positrons. In the present case, we tried to analyze the positron lifetime spectra in terms of such a component with 100% intensity but such a fit gave very poor variance of fit [7]. Owing to the presence of vacancy-type defects within the grains, as proved by the presently discussed trapping model analysis, it is clear that positron trapping occurred within the grains also, giving the characteristic and consistent values of τ_1 as listed in table 1. The question then arises as to where and how the lifetimes of positrons trapped in the vacancies of the Mn-doped samples are reflected. It may also be noted that at higher concentrations of doping, especially above 1 at.%, the positron lifetime τ_1 starts increasing (figure 4). I_2 also increases while S sharply decreases (figure 5). In order to explain this, the second situation of three-state positron trapping is considered [16]. Here the shorter lifetime τ_1 is considered well resolved and the longer lifetime τ_2 is assumed to consist of closely lying lifetimes of positrons annihilating in two different kinds of defect. The trapping model equation in this case takes the form [17]

$$\frac{1}{\tau_1^{cal}} = \frac{1}{\tau_f} + \kappa_{12}. \tag{2}$$

The sensitivity to the individual types of defect is lost and a cumulative trapping rate κ_{12} is calculated as

$$\kappa_{12} = \frac{\tau_m - \tau_f}{\tau_2 - \tau_m}\frac{1}{\tau_f} \tag{3}$$

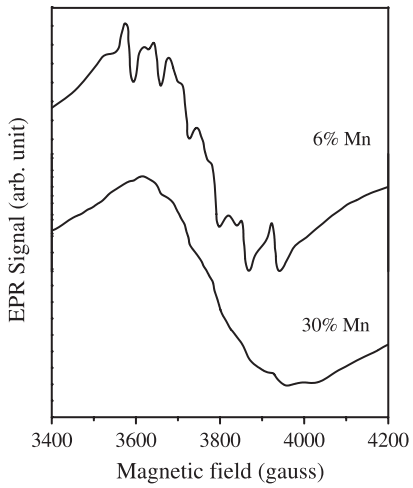

Figure 7. EPR spectra of the Mn-doped ZnS nanoparticles of two different Mn^{2+} concentrations.

where $\tau_m = (\tau_1 I_1 + \tau_2 I_2 + \tau_3 I_3)/(I_1 + I_2 + I_3)$ is the mean lifetime of positrons. For Mn^{2+} concentrations other than 0 and 30 at.% this model has satisfactorily reproduced the experimentally measured positron lifetimes (table 1). Thus it appears that the longer lifetime τ_2 is an admixture of the lifetimes of positrons annihilating in the grain surfaces as well as that in the vacancies within the nanocrystals.

At the highest concentration of 30 at.%, the Mn–Mn interaction becomes more effective, leading to the formation of Mn clusters. This has been verified from EPR measurements, as shown in figure 7. Typical six-line hyperfine structures appeared at the lower concentration of Mn^{2+}. At very low Mn^{2+} concentration, this spectral feature arose due to the $|-1/2\rangle$ to $|1/2\rangle$ transition coupled to Mn nuclear spin ($I = 5/2$) as a few Mn^{2+} ions isolated from each other were distributed inside the ZnS lattice. At the input concentration of 30 at.%, a dominant Lorentzian shaped spectrum was obtained due to the formation of Mn clusters. This could be the reason why the three-state trapping model (equation (1)) with a well-resolved τ_2 once again proved to be successful in defining the measured positron lifetimes (table 1). The fact that the Mn clusters could trap positrons is also indicated by a significantly higher value of I_2 at a concentration of 30 at.%, as shown in figure 4.

The two positron trapping rates κ_1 and κ_2 used in equation (1) are calculated as

$$\kappa_1 = \frac{\tau_1\left(\lambda_f - I_2\lambda_2\right) - I_1}{\tau_d - \tau_1} \tag{4}$$

and

$$\kappa_2 = \frac{I_2}{I_1}\left(\lambda_f - \lambda_2 + \kappa_1\right). \tag{5}$$

The saturation lifetime (τ_d) for the defects contributing to the trapping rate κ_1 is taken as the positron lifetime corresponding to monovacancies, i.e. 230 ps. The results of the calculations made using equations (3), (4) and (5) in the appropriate cases are summarized in figure 8. As explained above, there exist two trapping rate κ_1 and κ_2 for the undoped and the highest doped samples, whereas a cumulative trapping rate

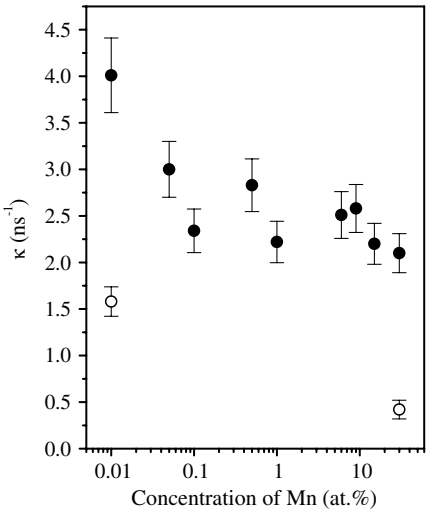

Figure 8. The positron trapping rates κ_1 (open circles) and κ_2 or κ_{12} (closed circles) in the ZnS nanoparticle samples at different concentrations of Mn doping. The data points corresponding to the undoped (x coordinate = 0) sample are shown against 0.01 at.%.

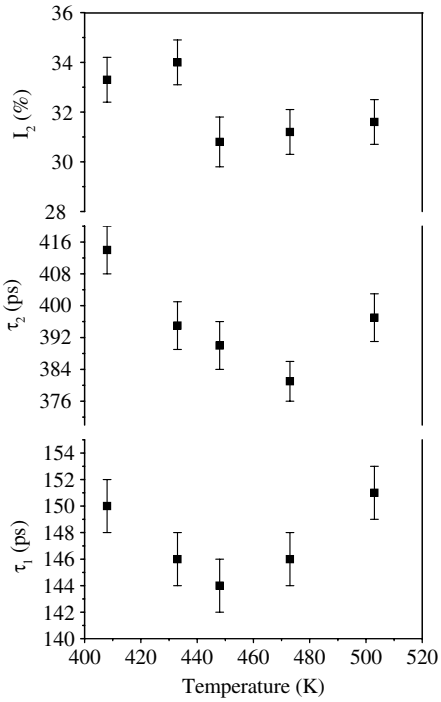

Figure 9. The variation of the positron lifetimes τ_1 and τ_2 and the intensity I_2 with the synthesis temperature of the Mn-doped ZnS nanoparticles.

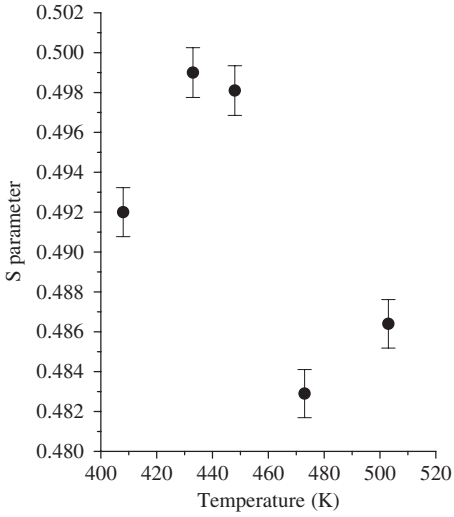

Figure 10. The variation of the S parameter with the synthesis temperature of the Mn-doped ZnS nanoparticles.

κ_{12} is plotted for the intermediate concentrations. The overall trend, nevertheless, is a gradually decreasing trapping effect. Notwithstanding the increase of I_2 at higher concentrations (figure 4), the defect concentration and hence the trapping rate decrease. Moreover, the annihilation at the grain surfaces might have decreased since more positrons are trapped by the Mn clusters (causing, in turn, an increase in I_2). It may also be noted that for an extremely high concentration of Mn^{2+} ions the large strain within the ZnS lattice might introduce additional lattice defects. These structural defect sites could also take part in the trapping of positrons.

The results of coincidence Doppler broadening measurements shown in figures 6(a), (b) and (c) help to illustrate these aspects further. With the inclusion of just 0.1 at.% Mn^{2+} ions, the peaks of the curves shift over to that of manganese, indicating that positrons are now able to directly annihilate with the core electrons of manganese and it necessarily implies that the sulfur vacancies are now able to trap positrons. This, however, will be possible only when the positive charge of the sulfur monovacancy is annulled by the opposite charge of a neighboring monovacancy of Zn. The initial increase of τ_2 may also suggest the formation of larger vacancy clusters and it can imply that neutral divacancies of neighboring zinc and sulfur ions are formed. In such a situation, the trapped positron can sense the substitution of the Zn^{2+} ion in the immediate neighborhood of the sulfur vacancy by the Mn^{2+} ion. The intensities of the area-normalized curves indicated that positrons in the sample with a Mn^{2+} concentration of 1 at.% (not shown in the figure) saw maximum Mn^{2+} ion concentrations and the intensity then dropped down owing perhaps to more of vacancies being recombined with the doped Mn^{2+} ions. At 30 at.%, however, the intensity increased once again due to the formation of Mn clusters, as indicated earlier by the sharp rise of the intensity I_2.

In another effort to look more closely at the role of Mn^{2+} ions on the mechanism of positron trapping in the ZnS nanocrystallites, we measured the positron lifetimes and lineshape parameter S for samples with a fixed input Mn^{2+} ion concentration (6 at.%) but with different synthesis temperatures. The results are illustrated in figures 9 and 10. The advantage of using higher synthesis temperatures is to provide additional energy to the Mn^{2+} ions to recombine with the Zn vacancy sites or substitute the Zn atoms in the ZnS lattice. This is in fact verified from the results of EDAX analysis, reported in figure 3. The actual intake of Mn^{2+} increases with increase in the synthesis temperature. The result is that an increasing number of vacancies are being occupied by

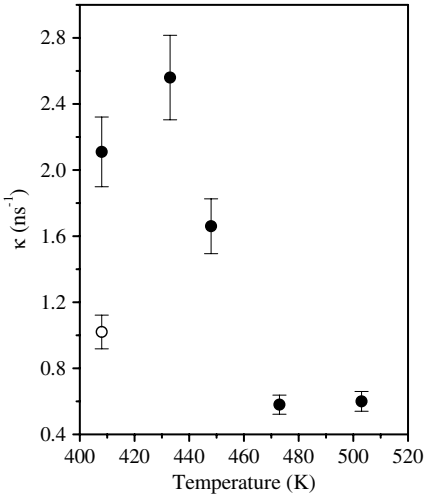

Figure 11. The positron trapping rates κ_1 (open circles) and κ_2 or κ_{12} (closed circles) in the ZnS nanoparticle samples as a function of the temperature of synthesis.

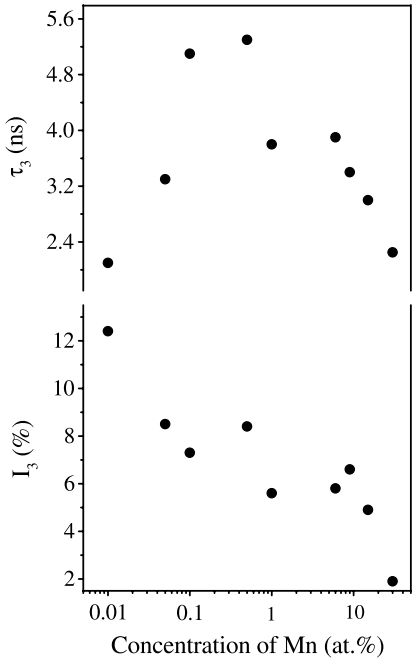

Figure 12. The orthopositronium lifetime τ_3 and intensity I_3 versus Mn^{2+} concentration of the ZnS nanoparticle samples. (The errors in the data points are less than their size.) The data points corresponding to the undoped (x coordinate = 0) sample are shown against 0.01 at.%.

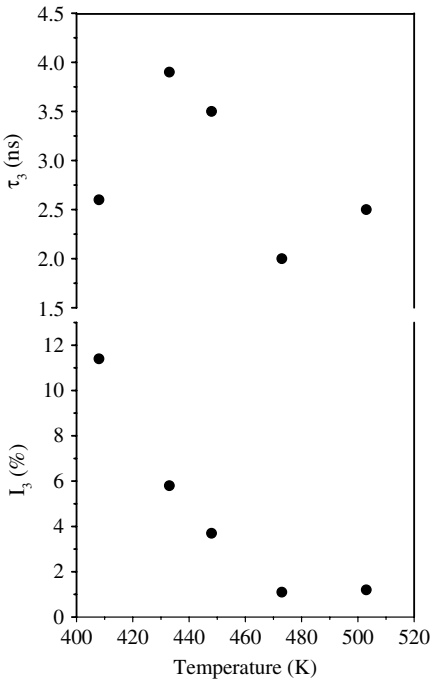

Figure 13. The orthopositronium lifetime τ_3 and intensity I_3 versus the temperature of synthesis of the samples. (The errors in the data points are less than their size.)

Mn^{2+} ions and the positron lifetimes τ_1 and τ_2 and the intensity I_2 decrease (figure 9). This is also reflected in a drastic fall of S, as shown in figure 10. The increasing temperature has also helped the grains to grow slightly in size from 2 to 7 nm, as estimated from the widths of the x-ray diffraction peaks. This will also reduce the positron lifetimes at the grain interfaces, since the fractional free volumes associated with the vacancies on the grain surfaces decrease with increasing grain size [15]. A further reason is the fact already stated earlier that 7 nm is on the higher side of the excitonic Bohr diameter of 5 nm for ZnS and the quantum confinement effects disappear, thereby reducing the positron lifetimes. At higher temperatures (448 K and above), the actual intake of Mn^{2+} increases further (figure 3) and increasing amounts of strain are being introduced in the lattice. This would activate the existing defects to agglomerate (feasibly with the increase in particle size) and accordingly the lifetime will increase (figure 9). The positron trapping rates, estimated by using equations (4) and (5) for the sample synthesized at 408 K and equation (3) for the other samples, fall drastically owing to the substantial occupation of Zn^{2+} vacancies by the increasing number of Mn^{2+} ions being incorporated into the lattice (figure 11). The CDBS results of figure 6(b) indicate again the increased annihilation with core electrons of manganese as more and more Mn^{2+} ions are becoming incorporated in the ZnS lattice.

The behavior of the positronium lifetimes and the intensities, τ_3 and I_3, in the two cases discussed is consistent with the arguments presented. As shown in figures 12 and 13, the intensity component decreases owing to decreasing open volume regions brought in by the increasing Mn^{2+} concentration. The variation of the lifetime can be explained as follows. In nanocrystalline materials, positronium formation is generally expected to take place in the intergranular region. Within the grains, however, positronium may be formed if the vacancy clusters are of sizes larger than the critical radius for its formation (∼1 Å) [18]. The standard formula available for the estimation of the cavity sizes from the measured positronium lifetime [19] suggests a defect radius varying from 2 to 2.5 Å for positronium atoms with lifetimes of 2.0–5.2 ns. Considering that the grain sizes here are about 2.5 nm, vacancy-type defects of such sizes are still physically

Table 2. Positron lifetimes and intensities in the ZnS sample of nanoparticles with average size 2 nm when the measurements were carried out in a vacuum and in air.

V.O.F.′	τ_1 (ps)	I_1 (%)	τ_2 (ps)	I_2 (%)	τ_3 (ns)	I_3 (%)	τ_4 (ns)	I_4 (%)
				In vacuum				
1.15	153 ± 2	55.1 ± 1.3	412 ± 1.3	28.3 ± 1.1	1.75 ± 0.10	6.6 ± 0.3	7.29 ± 0.11	10.0 ± 0.2
				In air				
1.12	161 ± 2	54.4 ± 1.1	422 ± 7	34.9 ± 1.0	1.91 ± 0.10	10.7 ± 0.1	—	—

′ Variance of fit in the positron lifetime data analysis.

feasible and may favor the formation of positronium. At higher concentration of Mn^{2+}, recombination takes place and the favored sites of positronium formation shift to the intergranular region. There the lifetimes of positronium atoms may be influenced by traces of Mn^{2+} ions lying in excess of the exact intake within the ZnS lattice. The decreasing intensity I_3 supports this argument. It may also be mentioned here that the decreasing trend of I_3 with increasing Mn^{2+} ion concentration or the temperature of synthesis in the respective cases has also significantly affected the overall behavior of the S parameter. This is to be expected, since the annihilation of positronium, the bound state of the electron with positron, will populate the peak region of the spectrum from which S is derived.

Finally, in discussing the formation and annihilation of positronium in the case of samples in powder form and composed of nanometer-sized particles, it is important to address the question of whether the said open volume defects are present inside or outside the nanoparticles. During all the measurements, the results of which we have discussed so far, the source–sample assembly was maintained in a good vacuum (10^{-3} mbar) in order to eliminate the possibility of positron trapping in air or other gases. To clarify this point, we performed positron lifetime and Doppler broadening measurements in one sample in both vacuum and air separately and the peak-normalized positron lifetime spectra are shown in figure 14. The resolved positron lifetimes and their intensities in the two cases are summarized in table 2. The average grain size of this sample was about 2 nm as estimated from the x-ray diffraction peak widths and expectedly the positron lifetimes, first measured with the sample in vacuum, were even higher than those shown in figures 9 and 13. In fact, a second positronium lifetime (τ_4) as long as 7.29 ns could be obtained with an appreciable intensity of 10.0% besides a lower 'pick-off' lifetime component τ_3 of 1.75 ns with 6.6% intensity. On the other hand, when measurements were carried out in air, the longest positronium component completely disappeared and the 'pick-off' lifetime τ_3 changed only marginally with an intensity of 10.7%. The shorter lifetimes τ_1 and τ_2 and their intensities (when normalized to $I_1 + I_2 + I_3 = 100\%$ in the case of measurements in vacuum) remained almost unchanged. This shows that a significant fraction of positrons indeed diffuse out to the surfaces of nanometer-sized grains and form positronium in the intergranular region and the positronium lifetime and intensity can be quenched by the presence of external gases. Further, the observation that the shorter lifetimes and their intensities are not significantly affected implies effective positron trapping by vacancy clusters within the grains. In other words, it offers proof of the presence

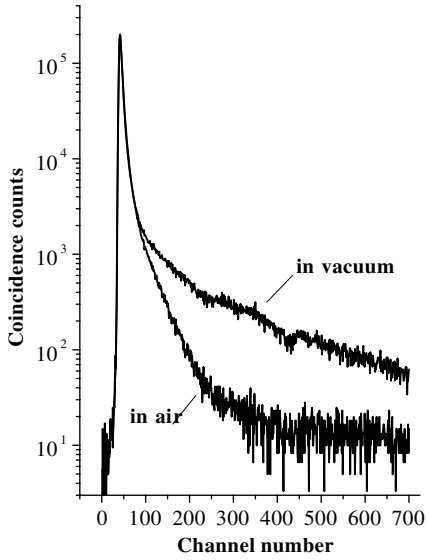

Figure 14. Peak-normalized positron lifetime spectra of a ZnS sample of nanoparticles with average size 2 nm when the measurements were carried out in a vacuum and in air.

of open volume defects inside the nanoparticles. The sharpness of the Doppler broadened lineshape of the spectrum recorded with the source–sample assembly in air is found to be reduced due to the quenching effect, as shown in figure 15, and the S parameter dropped by about 2.2% (i.e., $S_{\text{air}}/S_{\text{vacuum}} = 0.98$).

The results are strikingly different from our earlier observations of Mn-doped ZnS nanorods where the vacancies in the interior region of the nanorods became fully recombined with the addition of a small concentration of the dopant ions [6]. The two-state trapping model reproduced the experimentally measured τ_1 and the CDBS results gave no evidence of annihilation with electrons of manganese, suggesting that vacancy agglomeration did not occur. This indicates that positron annihilation measurements can be used to monitor even morphological changes in nanosystems up to a certain satisfactory extent.

4. Conclusions

In conclusion, we point out that the incorporation of Mn^{2+} ions as dopants in nanocrystalline ZnS gives rise to some interesting features which could be subjected to investigation by positron annihilation. The doping by Mn^{2+} ions results in the recombination of a fraction of the defects present within the particles. The driving force for this process is the strain being introduced due to the slightly higher ionic

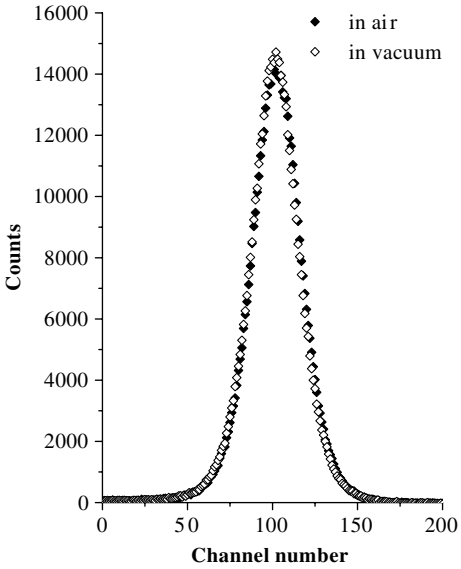

Figure 15. Doppler broadened gamma ray spectra of a ZnS sample of nanoparticles with average size 2 nm when the measurements were carried out in a vacuum and in air. The spectra are normalized for equal area under the curves.

radius of Mn^{2+} and is verified by measurements on samples synthesized at different temperatures. At higher concentrations of doping clusters of Mn are formed, which also trapped positrons. The results were also confirmed from coincidence Doppler broadening measurements, which has the virtue of identifying the elemental surroundings of positron trapping sites and therefore vividly displaying the annihilation with core electrons of manganese thereby implying the formation of clusters of neighboring vacancies during increased doping. Further it should be noted that, unlike the case of nanometer-sized grains of metals where almost all the positrons within the grains diffuse out to the surfaces before annihilation, there can be finite trapping probabilities for positrons within the grains of semiconductor nanomaterials owing to the presence of inherent non-stoichiometric defects in the crystalline structure. The presence of positron trapping defects within the nanoparticles and the diffusion of a fraction of positrons to the nanoparticle surfaces are verified by carrying out measurements in samples kept in a vacuum and air. While the lifetimes and intensities of positrons annihilating within the nanoparticles remained unchanged, those of positronium atoms formed in the intergranular region were significantly reduced, as indicated by a substantial drop in the sharpness of the Doppler broadened positron annihilation gamma ray spectrum as well.

Acknowledgment

The authors wish to express their thanks to Tandra Ghoshal of the Indian Association for the Cultivation of Sciences, Kolkata for help rendered by her during the experiments and discussion.

References

[1] Bhargava R N, Gaillagher D, Hong X and Nurmikko A 1994 *Phys. Rev. Lett.* **72** 416
[2] Sapra S, Nanda J, Anand A, Bhat S V and Sarma D D 2003 *J. Nanosci. Nanotechnol.* **3** 392
[3] Kar S, Biswas S, Chaudhuri S and Nambissan P M G 2005 *Phys. Rev.* B **72** 075338
[4] Biswas S, Kar S and Chaudhuri S 2005 *J. Phys. Chem.* B **109** 17526
[5] Biswas S, Kar S, Chaudhuri S and Nambissan P M G 2006 *J. Chem. Phys.* **125** 164719
[6] Kar S, Biswas S, Chaudhuri S and Nambissan P M G 2007 *Nanotechnology* **18** 225606
[7] Kirkegaard P, Eldrup M, Mogensen O E and Pedersen N J 1981 *Comput. Phys. Commun.* **23** 307
[8] Asoka-Kumar P, Alatalo M, Ghosh V J, Kruseman A C, Nielsen B and Lynn K G 1996 *Phys. Rev. Lett.* **77** 2097
[9] For detailed discussion, see Rehberg R K and Leipner H S 1999 *Positron Annihilation in Semiconductors—Defect Studies* (Berlin: Springer) pp 1–126
[10] Plazaola F, Seitsonen A P and Puska M J 1995 *Mater. Sci. Forum* **175–178** 469 (http://www.scientific.net/0-87849-686-6/469)
[11] Brunner S, Puff W, Balogh A G and Mascher P 1999 *Physica* B **273/274** 898
[12] Adams M, Mascher P and Kitai A H 1995 *Appl. Phys.* A **61** 217
[13] Bergersen B, Pajanne E, Kubica P, Stott M J and Hodges C H 1974 *Solid State Commun.* **15** 1377
[14] Urbaszek B, Townsley C M, Tang X, Morhain C, Balocchi A, Prior K A, Nicholas R J and Cavenett B C 2002 *Phys. Status Solidi* b **229** 549
[15] Chattopadhyay P P, Nambissan P M G, Pabi S K and Manna I 2001 *Phys. Rev.* B **63** 054107
[16] Bergersen B and Stott M J 1969 *Solid State Commun.* **7** 1203
[17] For a detailed discussion on different cases of positron trapping in solids, see Hautojarvi P and Corbel C 1995 *Positron Spectroscopy of Solids* (Amsterdam: IOS Press) pp 491–532
[18] Uedono A, Sadamoto R, Kawano T, Tanigawa S and Uryu T 1995 *J. Polym. Sci.* B **33** 891
[19] Nakanishi H, Wang S J and Jean Y C 1988 *Positron Annihilation Studies of Fluids* ed S C Sharma (Singapore: World Scientific) p 292